



Effects of initial δ phase (Ni_3Nb) on hot tensile deformation behaviors and material constants of Ni-based superalloy

Yong-cheng LIN^{1,2,3}, Min HE^{1,3}, Ming-song CHEN^{1,3}, Dong-xu WEN^{1,3}, Jian CHEN⁴

1. School of Mechanical and Electrical Engineering, Central South University, Changsha 410083, China;

2. Light Alloy Research Institute, Central South University, Changsha 410083, China;

3. State Key Laboratory of High Performance Complex Manufacturing,
Central South University, Changsha 410083, China;

4. Key Laboratory of Efficient and Clean Energy Utilization, School of Energy and Power Engineering,
Changsha University of Science and Technology, Changsha 410114, China

Received 10 June 2015; accepted 11 October 2015

Abstract: Effects of initial δ phase (Ni_3Nb) on the hot tensile deformation behaviors and material constants of a Ni-based superalloy were investigated over wide ranges of strain rate and deformation temperature. It is found that the true stress–true strain curves exhibit peak stress at a small strain, and the peak stress increases with the increase of initial δ phase. After the peak stress, initial δ phase promotes the dynamic softening behaviors, resulting in the decreased flow stress. An improved Arrhenius constitutive model is proposed to consider the synthetical effects of initial δ phase, deformation temperature, strain rate, and strain on hot deformation behaviors. In the improved model, material constants are expressed as the functions of the content of initial δ phase and strain. A good agreement between the predicted and measured results indicates that the improved Arrhenius constitutive model can well describe hot deformation behaviors of the studied Ni-based superalloy.

Key words: Ni-based superalloy; hot deformation; initial δ phase; constitutive model; material constants

1 Introduction

Hot deformation of metals or alloys is extensively performed in the manufacture of products with desired geometry and required properties [1,2]. Generally, hot deformation behaviors are significantly influenced by the thermo-mechanical parameters, such as deformation temperature, strain rate and strain [3,4]. Meanwhile, several deformation mechanisms, such as the work hardening (WH) [5], dynamic recovery (DRV) [6] and dynamic recrystallization (DRX) [7], often occur and result in complex microstructural evolution during hot deformation. Therefore, understanding the hot deformation behaviors of metals or alloys has a great importance for designers to optimize the hot forming process and guarantee the final mechanical properties of products.

In order to optimize the hot forming process, many investigators have studied the hot deformation behaviors of metals or alloys. Some excellent constitutive models are developed to describe the plastic deformation behaviors of metals or alloys. LIN and CHEN [1] presented a critical review on constitutive models for metals or alloys under hot working. Constitutive model expressed by Arrhenius hyperbolic-sine function has been widely applied to investigating the effects of thermo-mechanical parameters on hot deformation behaviors of metals or alloys. Considering the effects of strain on material parameters, LIN et al [8] proposed a revised Arrhenius constitutive model to describe the deformation behaviors of 42CrMo steel over wide ranges of deformation temperature and strain rate. Furthermore, this constitutive model has been extensively verified to be suitable for some other alloys, such as typical steels [9–11], aluminum alloy [12–14], magnesium

Foundation item: Projects (51375502, 51305466) supported by the National Natural Science Foundation of China; Project (2015CX002) supported by the Innovation-driven Plan in Central South University, China; Project (2013CB035801) supported by the National Basic Research Program of China; Project (2015NGQ001) supported by Key Laboratory of Efficient & Clean Energy Utilization, College of Hunan Province, China

Corresponding author: Yong-cheng LIN; Tel: +86-13469071208; E-mail: yclin@csu.edu.cn

DOI: 10.1016/S1003-6326(15)64043-2

alloys [15–17], and some other alloys [18]. In addition, HE et al [19], SALARI et al [20], ABBASI-BANI et al [21], LI et al [22], and LIN et al [23] successfully modified Johnson–Cook models to describe hot deformation behaviors of different alloys. Also, SHAMSOLHODAEI et al [24], HE et al [25], CHAI et al [26], and SAMANTARAY et al [27] successfully improved Zerilli–Armstrong model to predict flow stresses of metals or alloys. Based on the classical stress–dislocation relation and dynamic recrystallization kinetics, LIN et al [28,29], JI et al [30], SAJADIFAR and YAPICI [31], and LIANG et al [32] developed physical-based constitutive models to describe the work hardening–dynamic recovery and dynamic recrystallization behaviors of some alloys.

Due to the excellent mechanical properties and good corrosion resistance under elevated temperature, Ni-based superalloys are widely used in gas turbines and aerospace engines [33,34]. Ni-based superalloys are precipitation strengthening alloys, and the major strengthening phases are γ'' (Ni_3Nb) and γ' (Ni_3Al) precipitates. Additionally, the metastable γ'' phase can transform to the equilibrium δ phase (Ni_3Nb) within the suitable temperature range [35,36]. Previous studies show that the effects of δ phase on microstructural evolution and hot deformation behaviors of Ni-based superalloys are obvious and complex [5,37–40]. Although some efforts have been invested into hot compressive deformation behaviors of Ni-based superalloy [41,42], the effects of initial δ phase on hot tensile deformation behaviors and material constants are still necessary to be further investigated.

In this study, the effects of initial δ phase on hot deformation behaviors are investigated by uniaxial tensile tests over wide ranges of deformation temperature and strain rate. An improved Arrhenius constitutive model involving the content of initial δ phase is proposed to describe the hot deformation behaviors of the studied Ni-based superalloy. Also, the effects of initial δ phase on the apparent deformation activation energy are discussed.

2 Experimental

A typical Ni-based superalloy with the chemical composition (mass fraction) of 52.82%Ni–18.96%Cr–5.23%Nb–3.01%Mo–1.00%Ti–0.59%Al–0.01%Co–0.03%C, balance Fe was used in this investigation. According to ISO 6892-2 [43], the specimens with the gauge length of 30 mm and the diameter of 5 mm were machined from the as-received wrought billet (Fig. 1). The specimens were solution-treated in 1040 °C for 45 min, and subsequently cooled to room temperature in the air. In order to investigate the effects of initial δ

phase on hot deformation behaviors of the studied Ni-based superalloy, the solution-treated specimens were separately aged for 8, 12 and 24 h at 900 °C, and then cooled to room temperature in air. The microstructures of the solution-treated and aged specimens were observed by an optical microscopic (OM). The metallography specimens were chemically etched with a solution consisting of 5 g CuCl_2 +100 mL HCl + 100 mL $\text{C}_2\text{H}_5\text{OH}$ at room temperature for 3–5 min.

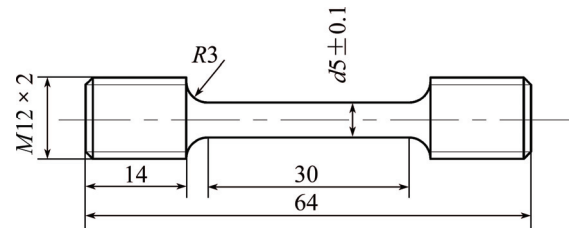


Fig. 1 Dimensions for uniaxial hot tensile specimens (unit: mm)

Uniaxial tensile tests were carried out at deformation temperatures of 920, 950, 980 and 1010 °C, and constant tensile speeds of 0.3, 0.15 and 0.03 mm/s (i.e., initial strain rates of 0.01, 0.005, and 0.001 s^{-1}). Prior to loading, the specimens were heated to the deformation temperature at the heating rate of 10 °C/min, and held for 30 min to eliminate thermal gradient. The fluctuation of temperature was controlled within 1 °C. The hot tensile tests were conducted in a constant tensile speed until failure on MTS-GWT2105 test machine. Finally, the fractured specimens were cooled to room temperature in the furnace.

3 Results and discussion

3.1 Microstructures of solution-treated and aged superalloys

Figure 2 shows the effects of heat treatment processing on the optical microstructures of the studied Ni-based superalloy. It can be found that there are no obvious changes in grain size after all the heat treatments, and the mean grain size is evaluated as about 75 μm by the linear intercept method [38]. However, the morphologies and contents of δ phase are significantly affected by heat treatment processing. As shown in Fig. 2(a), for the solution-treated material, the microstructure is mainly composed of fine equiaxed grains and clean grain boundaries without δ phase, and a substantial amount of straight annealing twins can be found. When the aging time is 8 h (Fig. 2(b)), there are two morphologies of δ phases. The dominant morphologies are short needle-shaped which distribute at grain boundaries, and only a small number of spherical δ phases precipitate within grains. As the aging time is

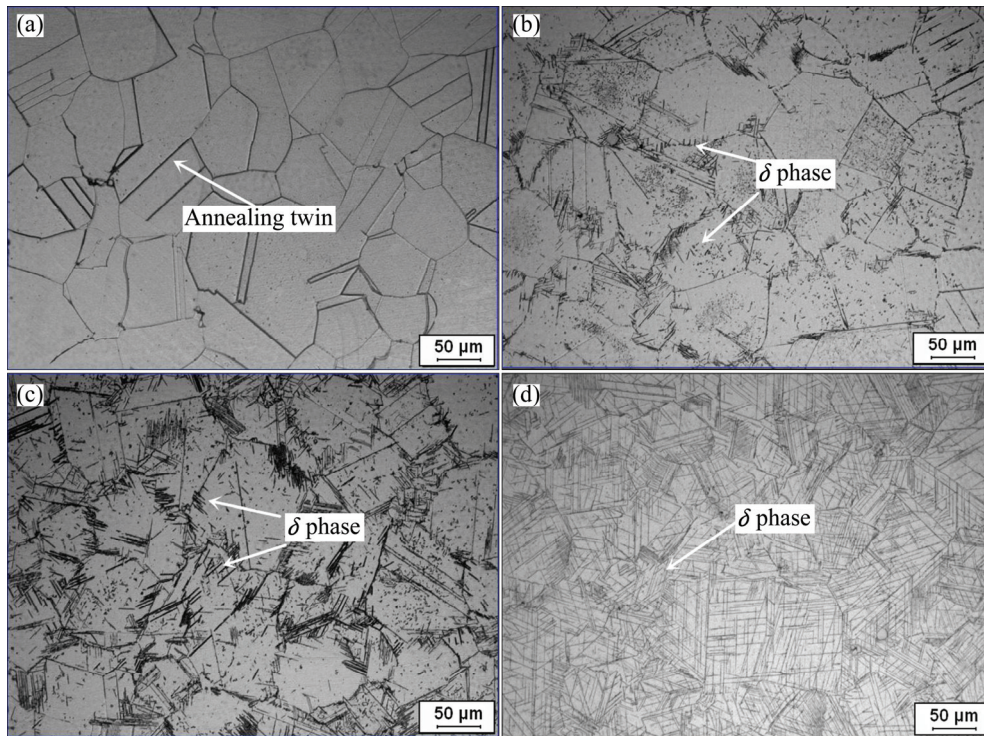


Fig. 2 Initial optical microstructures of studied Ni-based superalloy: (a) Solution-treated; (b) Aged for 8 h; (c) Aged for 12 h; (d) Aged for 24 h

increased to 12 h (Fig. 2(c)), the short needle-shaped δ phases extend from grain boundaries into grain interior. Meanwhile, the spherical δ phases transform to the needle-shaped ones within grains. When the aging time is continuously increased to 24 h, a great number of long needle-shaped δ phases uniformly distribute in the matrix, as shown in Fig. 2(d). From Fig. 2, it can also be found that the content of δ phase increases with the increase of aging time. Generally, the precipitation of δ phase is considered as a diffusion-controlled process, and the increase of aging time promotes the nucleation and growth of precipitates. In order to quantitatively analyze the effects of initial δ phase on hot deformation behavior, the contents of initial δ phase were evaluated by the Image-Pro Plus software. Ten different images via optical microstructures for each specimen were analyzed, and the average contents of initial δ phase of the specimens aged for 8, 12, and 24 h can be evaluated as 4.96%, 7.80% and 12.09%, respectively. The detailed procedures to evaluate the content of δ phase can be seen in Ref. [44].

3.2 Correction of true stress–true strain curves

It is well known that the true stress–true strain curve of metals under constant strain rate is very important to analyze the hot deformation behavior. However, as mentioned in Section 2, the uniaxial tensile tests were performed under constant tensile speed. In order to obtain the true stress–true strain curves under

constant strain rate, it is necessary to correct the experimental curves measured by constant speed tensile tests.

The tensile deformation often consists of three distinct stages, i.e., uniform deformation, diffusion necking and localized necking, and the specimen exhibits macroscopic uniform deformation before localized necking [37]. Therefore, the true stress–true strain before localized necking can be evaluated by

$$\varepsilon = \ln(l/l_0) \quad (1)$$

$$\sigma = \frac{F}{A_0} e^{\varepsilon} \quad (2)$$

where A_0 is the initial cross-sectional area of specimen, l_0 is the initial gauge length of specimen, l is the instantaneous gauge length of specimen, F is the deformation resistance, ε is the true strain, and σ is the true stress. From Eqs. (1) and (2), the true stress–true strain under constant tensile speed can be obtained.

In addition, the instantaneous strain rate can be usually evaluated by

$$\dot{\varepsilon} = v/l \quad (3)$$

where $\dot{\varepsilon}$ and v are the strain rate and tensile speed, respectively.

During the uniaxial tensile tests, the instantaneous gauge length of specimen (l) gradually increases. Therefore, according to Eq. (3), the instantaneous strain

rate decreases with the further deformation. In this work, a new method is proposed to correct the true stress–true strain curves under constant strain rate from the experimental curves measured by constant speed tensile tests. Taking the solution-treated superalloy as an example, the followings introduce the correction procedure for the flow stress under the deformation temperature of 980 °C and true strain of 0.1. According to the Hollomon equation, the flow stress can be expressed as

$$\sigma = K \dot{\varepsilon}^m \varepsilon^n \exp[Q/(RT)] \quad (4)$$

where K is material constant, m is the strain rate sensitivity coefficient, n is strain hardening exponent, R is the mole gas constant, T is the temperature, and Q is the apparent activation energy. Taking the logarithm of both sides of Eq. (4) gives

$$\ln \sigma = \ln K + m \ln \dot{\varepsilon} + n \ln \varepsilon + Q/(RT) \quad (5)$$

Based on the experimental data, the true stress (Eq. (2)) and instantaneous strain rate (Eq. (3)) can be evaluated under the deformation temperature of 980 °C and true strain of 0.1. Then, the relationship between the true stress and strain rate can be easily obtained, as shown in Fig. 3. Also, the value of m can be computed as 0.2147 from the slope of the linear fitting line in $\ln \sigma - \ln \dot{\varepsilon}$ plot. Finally, the corrected true stresses under constant strain rates (0.01, 0.005, 0.001 s⁻¹) can be evaluated, as shown in Table 1. Similarly, the correction of flow stress can be done for several strain levels, which are selected within 0.05–0.4 with the interval of 0.05. Therefore, the true stress–true strain curves under constant strain rates can be obtained, as shown in Fig. 4.

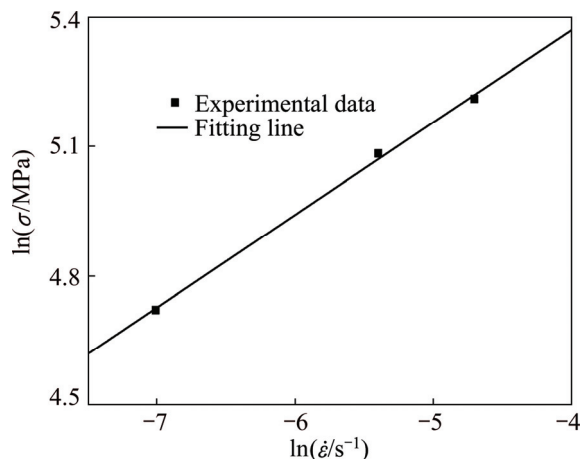


Fig. 3 Relationship between true stress and strain rate (deformation temperature: 980 °C; true strain: 0.1)

3.3 Hot deformation behaviors of studied Ni-based superalloy

In this section, the effects of deformation temperature, strain and strain rate on hot deformation

Table 1 Corrected true stress under deformation temperature of 980 °C and true strain of 0.1

Instantaneous strain rate/s ⁻¹	Experimental true stress/MPa	Constant strain rate/s ⁻¹	Corrected true stress/MPa
0.0090	183.155	0.01	187.131
0.0045	161.286	0.005	164.787
0.0009	112.271	0.001	114.708

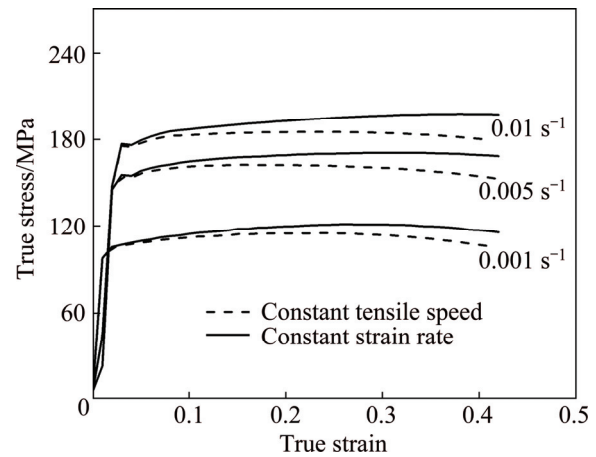


Fig. 4 True stress–true strain curves under constant tensile speed and constant strain rate (deformation temperature: 980 °C)

behaviors of the solution-treated superalloy is firstly discussed. Figure 5 shows the typical true stress–true strain curves of the solution-treated Ni-based superalloy before the localized necking. From Figs. 4 and 5, it can be easily found that the hot deformation behavior is sensitive to the deformation temperature, strain and strain rate. With the decrease of deformation temperature and increase of strain rate, the flow stress significantly increases. In the early deformation stage, the flow stress sharply increases at a very small strain, showing a typical elastic deformation. With the further straining, the yield

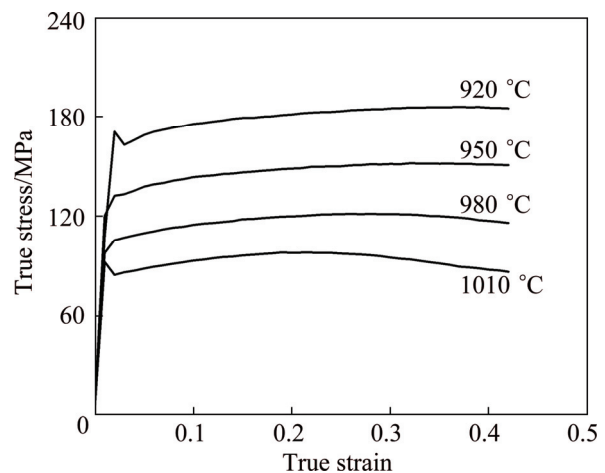


Fig. 5 True stress–true strain curves of solution-treated superalloy under strain rate of 0.001 s⁻¹

stress is reached which indicates that the plastic deformation occurs. In the plastic deformation stage, the hot deformation behavior shows different characteristics under the tested deformation conditions. Due to the work hardening–dynamic recovery, the hot deformation behaviors show the gradual increase of flow stress or a long steady stress stage at low deformation temperature [5]. When the deformation temperature is 1010 °C, the high deformation temperature provides sufficient energy for grain boundary mobility, which stimulates the dynamic recrystallization process [45–47]. Therefore, the hot deformation behaviors show the dynamic softening phenomenon at high deformation temperature.

Figure 6 shows the effects of initial δ phase on the true stress–true strain curves of the studied Ni-based superalloy at 950 °C and 0.001 s⁻¹. It can be found that the peak stress increases with the increase of initial δ phase. This is because that δ phase can impede the dislocation slip and enhance the resistance of dislocation movement. After the peak stress, the flow stress of solution-treated superalloy maintains a relatively steady value, while those of the aged superalloys decrease monotonically. Besides, the increase of initial δ phase accelerates the decrease of flow stress. This is because that δ phase promotes dynamic recrystallization process. Meanwhile, the initial δ phase is the nucleus for the formation of microvoids, and promotes the nucleation of microvoids [38].

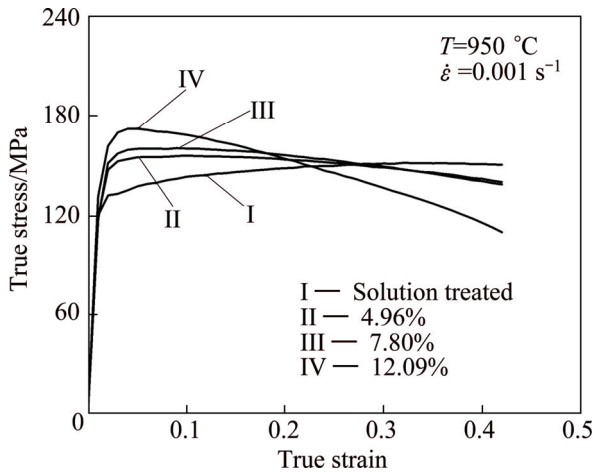


Fig. 6 True stress–true strain curves of studied Ni-based superalloy with different initial δ phase contents

3.4 Constitutive model for hot deformation behaviors

The Arrhenius constitutive model is widely used to describe the correlations between the flow stress, deformation temperature and strain rate. Furthermore, the effects of the temperature and strain rate on the deformation behaviors can be represented by Zener–Hollomon parameter (Z) in an exponent-type function. The hyperbolic-sine law in Arrhenius constitutive model

can give better approximations between Zener–Hollomon parameter and flow stress [1].

$$Z = \dot{\epsilon} \exp[Q/(RT)] \quad (6)$$

$$\dot{\epsilon} = AF(\sigma) \exp[-Q/(RT)] \quad (7)$$

where

$$F(\sigma) = \begin{cases} \sigma^{n'}, & \alpha\sigma < 0.8 \\ \exp(\beta\sigma), & \alpha\sigma > 1.2 \\ [\sinh(\alpha\sigma)]^n, & \text{for all } \sigma \end{cases} \quad (8)$$

where $\dot{\epsilon}$ is the strain rate (s⁻¹), A , n' , α , β and n are material constants, $\alpha = \beta/n'$.

3.4.1 Determination of material constants

According to the above analysis, initial δ phase significantly affects the flow stress of the studied Ni-based superalloy. In order to accurately predict the flow stress, the effects of initial δ phase on the material constants of Arrhenius constitutive model should be considered. In the following sections, taking the solution-treated superalloy as an example, the procedure to determine material constants is introduced under the true strain of 0.1.

For the low stress level ($\alpha\sigma < 0.8$) and high stress level ($\alpha\sigma > 1.2$), Eq. (7) can be expressed as

$$\dot{\epsilon} = B\sigma^{n'} \quad (9)$$

$$\dot{\epsilon} = B' \exp(\beta\sigma) \quad (10)$$

where B and B' are material constants, which are independent on deformation temperature. Taking the logarithm of both sides of Eqs. (9) and (10), respectively, we have

$$\ln \sigma = -\ln B/n' + \ln \dot{\epsilon}/n' \quad (11)$$

$$\sigma = -\ln B'/\beta + \ln \dot{\epsilon}/\beta \quad (12)$$

Based on the experimental results, the relationships between the flow stress and strain rate can be easily obtained, as shown in Fig. 7. Then, the averaged values of n' and β can be evaluated from the slopes of the parallel straight lines in $\ln \sigma - \ln \dot{\epsilon}$ and $\sigma - \ln \dot{\epsilon}$ plots, respectively. Furthermore, the averaged values of n' and β can be computed as 4.776 and 0.02974 MPa⁻¹, respectively. So, $\alpha = \beta/n' = 0.0062$ MPa⁻¹.

For all the stress levels, Eq. (7) can be represented as

$$\dot{\epsilon} = A[\sinh(\alpha\sigma)]^n \exp[-Q/(RT)] \quad (13)$$

Taking the logarithm of both sides of Eq. (13) gives

$$\ln[\sinh(\alpha\sigma)] = \frac{\ln \dot{\epsilon}}{n} + \frac{Q}{RTn} - \frac{\ln A}{n} \quad (14)$$

Substituting the deformation temperatures, strain rates and flow stresses into Eq. (14) gives the

relationships of $\ln[\sinh(\alpha\sigma)] - \ln \dot{\varepsilon}$ and $\ln[\sinh(\alpha\sigma)] - 1000/T$, as shown in Fig. 8. Then, the averaged values of material constants A , n and activation energy (Q) can be evaluated as $2.227 \times 10^{14} \text{ s}^{-1}$, 3.552 and 406.325 kJ/mol, respectively.

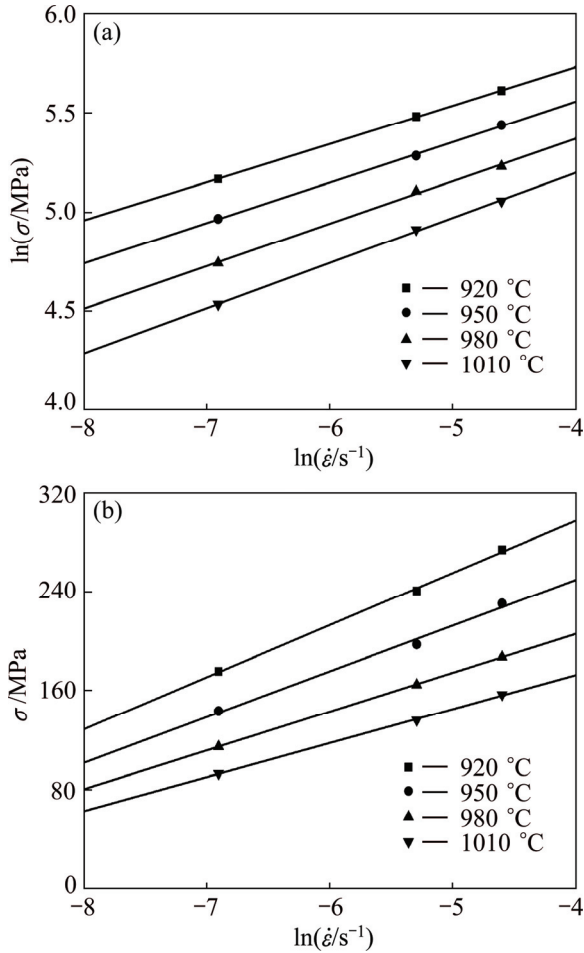


Fig. 7 Relationships between flow stress and strain rate: (a) $\ln \sigma$ and $\ln \dot{\varepsilon}$; (b) σ and $\ln \dot{\varepsilon}$ (symbols for experimental results; solid lines for fitting line)

Similarly, the material constants (α , n , A and Q) of Arrhenius constitutive model can be evaluated for the studied Ni-based superalloy with different initial contents of δ phase. Meanwhile, considering the effects of strain on material constants [8], the true strains are selected within 0.06–0.42 with the interval of 0.04. Finally, the relationships among material constants (α , n , A and Q), strain (ε) and initial content of δ phase (V) can be obtained, as shown in Fig. 9. It can be found that the strain and initial content of δ phase significantly affect the material constants of Arrhenius constitutive model. Therefore, the effects of strain and initial content of δ phase on material constants should be taken into account when Arrhenius constitutive model is established for the studied Ni-based superalloy.

It is well known that the compensation of strain in Arrhenius constitutive model can be incorporate by such

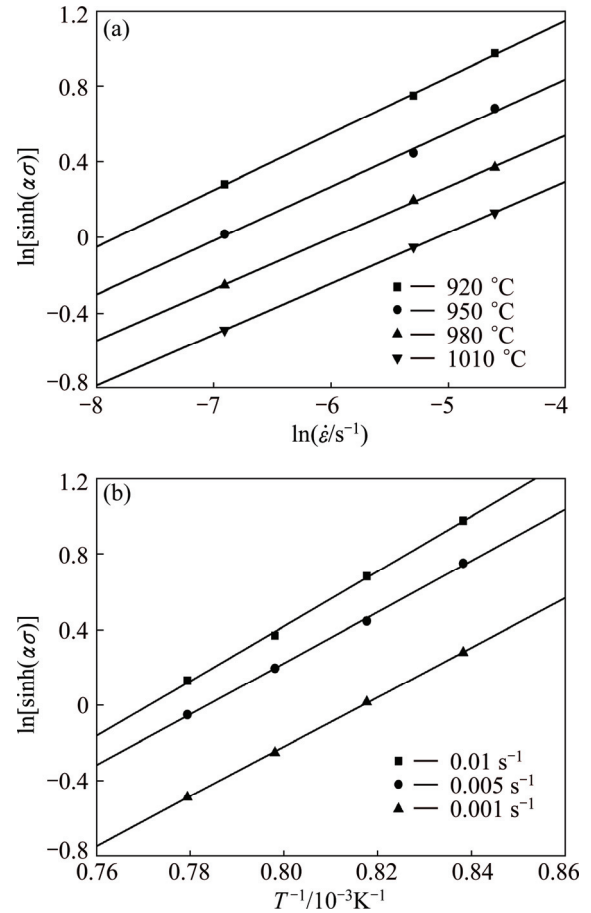


Fig. 8 Relationships between $\ln[\sinh(\alpha\sigma)]$ and $\ln \dot{\varepsilon}$ (a), $\ln[\sinh(\alpha\sigma)]$ and $1000/T$ (b) (symbols for the experimental results; solid lines for the fitting line)

an assumption that material constants are polynomial functions of strain [8]. However, in the present study, the effects of strain and initial content of δ phase on material constants are too complex to be expressed as a simple polynomial function. Therefore, Eq. (15) is proposed to describe the relationships among material constants, strain and initial content of δ phase.

$$\lambda = X_1 M^T + P X_2 P^T \quad (15)$$

where, $M = [1, \varepsilon, V]$, $P = [\varepsilon, V]$, $X_1 = [a, b, c]$,

$$X_2 = \begin{pmatrix} d + e\varepsilon & f + g\varepsilon \\ f + hV & i + jV \end{pmatrix}. \lambda \text{ represents material constants}$$

(α , n , $\ln A$ and Q), ε is strain, and V is initial content of δ phase. Additionally, other parameters (a , b , c , d , e , f , g , h , i and j) can be obtained by the nonlinear fitting method, and the details for α , n , $\ln A$ and Q are listed in Table 2.

After the material constants of Arrhenius constitutive model are determined, the flow stress can be predicted for the superalloys with different initial contents of δ phase. According to Eqs. (6) and (13), the flow stress can be written as a function of Zener–Hollomon parameter, and the established

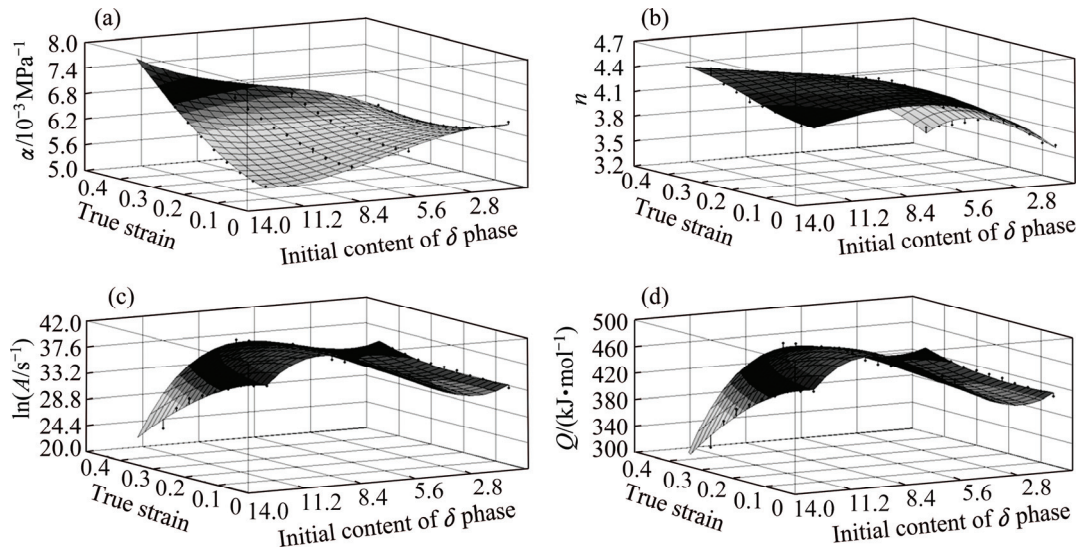


Fig. 9 Effects of strain and initial content of δ phase on material constants: (a) α ; (b) n ; (c) $\ln A$; (d) Q

constitutive model can be summarized as

$$\left\{ \begin{aligned} \sigma &= \frac{1}{\alpha} \ln \left(\left(\frac{Z}{A} \right)^{1/n} + \left(\left(\frac{Z}{A} \right)^{2/n} + 1 \right)^{1/2} \right) \\ Z &= \dot{\varepsilon} \exp[Q/(RT)] \\ \alpha &= \left\{ [6.604, -4.635, -0.006][1, \varepsilon, V]^T + \right. \\ &\quad \left. [\varepsilon, V] \begin{pmatrix} 9.492 - 4.559\varepsilon & 0.202 + 0.148\varepsilon \\ 0.202 + 0.005V & -0.025 + 0.001V \end{pmatrix} [\varepsilon, V]^T \right\} \times 10^{-3} \\ n &= [3.475, 0.941, 0.204][1, \varepsilon, V]^T + \\ &\quad \left. [\varepsilon, V] \begin{pmatrix} 1.815 - 9.699\varepsilon & -0.131 + 0.489\varepsilon \\ -0.131 + 0.010V & -0.018 + 0.0004V \end{pmatrix} [\varepsilon, V]^T \right. \\ \ln A &= [33.559, -4.965, -2.009][1, \varepsilon, V]^T + \\ &\quad \left. [\varepsilon, V] \begin{pmatrix} 8.855 + 21.349\varepsilon & 2.466 - 6.805\varepsilon \\ 2.466 - 0.394V & 0.660 - 0.039V \end{pmatrix} [\varepsilon, V]^T \right. \\ Q &= [412.647, -61.455, -21.299][1, \varepsilon, V]^T + \\ &\quad \left. [\varepsilon, V] \begin{pmatrix} 127.928 + 167.934\varepsilon & 27.795 - 75.833\varepsilon \\ 27.795 - 4.320V & 6.896 - 0.404V \end{pmatrix} [\varepsilon, V]^T \right. \end{aligned} \right. \quad (16)$$

3.4.2 Verification of developed constitutive model

In order to verify the improved constitutive model of the studied Ni-based superalloy, the comparisons between the measured and predicted results are carried out. Figure 10 shows the measured and predicted flow stress curves of the studied Ni-based superalloy under all the tested conditions. It can be found that the predicted flow stresses agree well with the measured ones. In order to further confirm the excellent prediction accuracy of the improved constitutive model, the correlation coefficient (R) and average absolute relative error

Table 2 Polynomial fitting results of α , n , $\ln A$ and Q for studied Ni-based superalloy

	$\alpha/10^{-3}\text{MPa}^{-1}$	n	$\ln(A/s^{-1})$	$Q/(kJ\cdot\text{mol}^{-1})$
<i>a</i>	6.604	3.475	33.559	412.647
<i>b</i>	-4.635	0.941	-4.965	-61.455
<i>c</i>	-0.006	0.204	-2.009	-21.299
<i>d</i>	9.492	1.815	8.855	127.928
<i>e</i>	-4.559	-9.699	21.349	167.934
<i>f</i>	0.202	-0.131	2.466	27.795
<i>g</i>	0.148	0.489	-6.805	-75.833
<i>h</i>	0.005	0.010	-0.394	-4.320
<i>i</i>	-0.025	-0.018	0.660	6.896
<i>j</i>	0.001	0.0004	-0.039	-0.404

(AARE) between the predicted and measured flow stresses are evaluated, respectively [28].

$$R = \frac{\sum_{i=1}^N (E_i - \bar{E})(P_i - \bar{P})}{\sqrt{\sum_{i=1}^N (E_i - \bar{E})^2 \sum_{i=1}^N (P_i - \bar{P})^2}} \quad (17)$$

$$\text{AARE} = \frac{1}{N} \sum_{i=1}^N \left| \frac{E_i - P_i}{E_i} \right| \times 100\% \quad (18)$$

where E_i and P_i are the measured and predicted flow stresses, respectively; \bar{E} and \bar{P} are the mean values of E_i and P_i , respectively; N is the total number of data used in this study. The correlation coefficient (R) is commonly employed as the statistical parameter and provides information regarding the strength of linear relationship between the measured and predicted values. The average absolute relative error is computed through a term by term comparison of the relative error

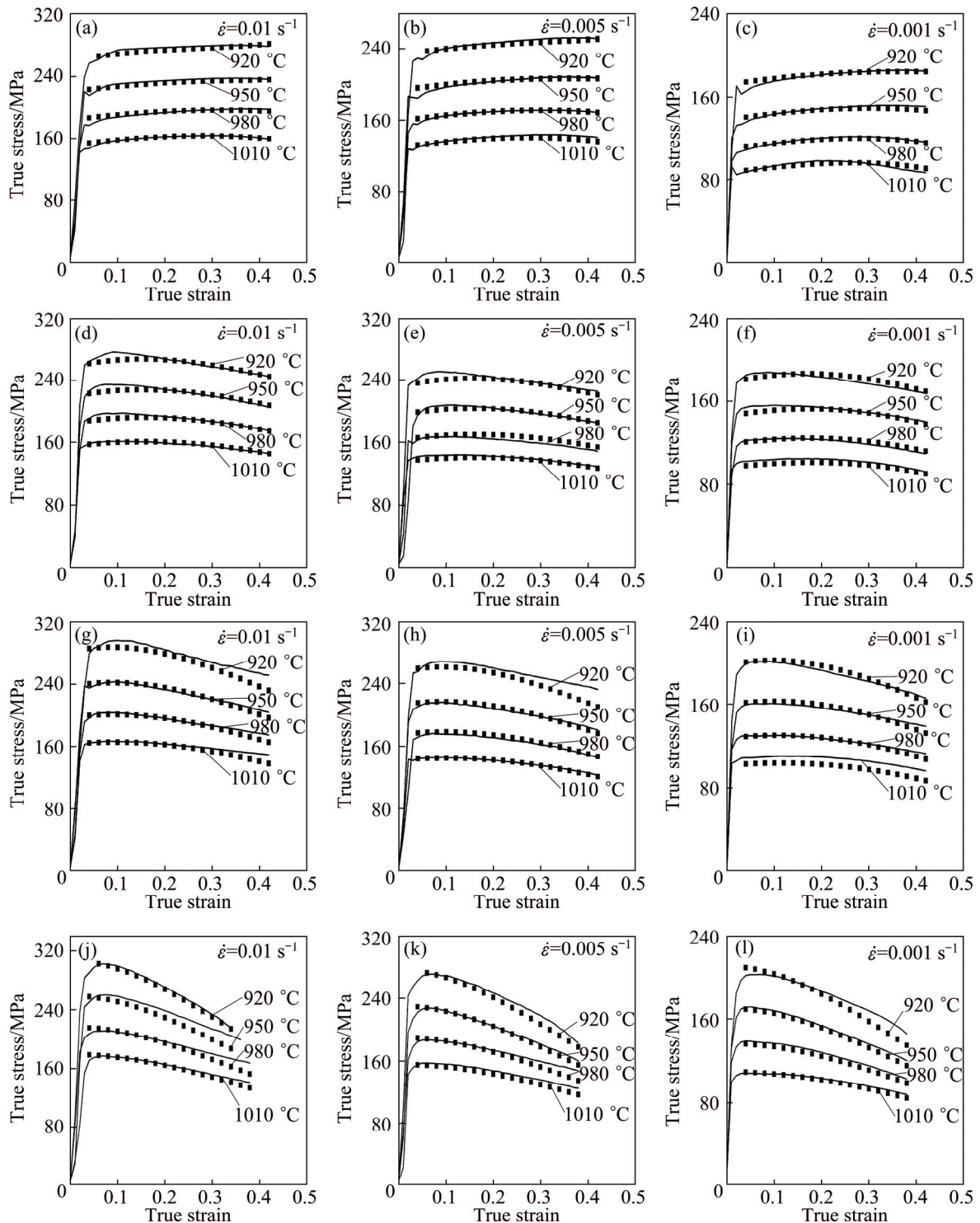


Fig. 10 Comparisons between measured and predicted flow stress curves under all tested conditions with different initial δ phase contents: (a–c) 0; (d–f) 4.96%; (g–i) 7.80%; (j–l) 12.09%

and therefore is an unbiased statistical parameter to further evaluate the predictability of model. Figure 11 shows the correlations between the measured and predicted flow stresses. It can be easily found that the correlation coefficient (R) and the average absolute relative errors are 0.993 and 1.75%, respectively, which reflects an excellent capability of the improved

constitutive model to describe the flow behaviors.

3.5 Effects of initial δ phase on apparent activation energy

According to the hot deformation theory, the activation energy represents the magnitude of the energy barrier which the atomic transition needs to overcome.

Therefore, the activation energy has been regarded as an important phenomenological parameter to reflect the workability of metals or alloys during hot deformation. Figure 12 shows the effects of initial δ phase on apparent activation energy. It can be found that the apparent activation energy weakly depends on the true strain, except for the superalloy with initial δ phase of 12.09%. The apparent activation energy (Q) is found in the range of 403.3–480.4 kJ/mol for the studied Ni-based superalloy. However, the apparent activation energy of the studied Ni-based superalloy is significantly higher than that of Ni self-diffusion (278 kJ/mol [48]). It is well known that the dynamic recrystallization is the major softening mechanism during hot deformation, and it is a thermal activation process. Such high apparent activation energy may attribute to dynamic recrystallization [2,28,49]. Besides, the apparent activation energy increases with the increase of initial δ phase. This is because the δ phase promotes the dislocation accumulation, which stimulates dislocation pile-up and the formation of cellular structure [5]. The cellular structure impedes the migration of dislocation and results in the increase of apparent activation energy.

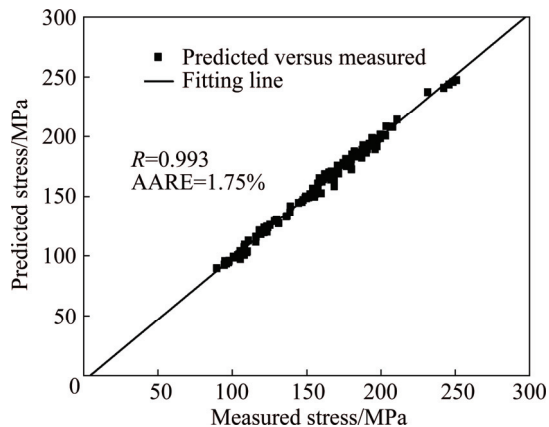


Fig. 11 Correlation between measured and predicted flow stresses

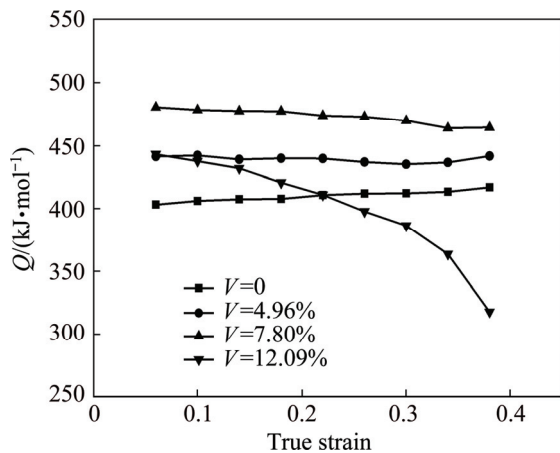


Fig. 12 Effects of strain and initial content of δ phase on apparent activation energy

From Fig. 12, it can also be found that the apparent activation energy decreases with the increase of strain when the initial content of δ phase is 12.09%. This phenomenon may result from the evolution of δ phase during hot deformation. Figure 13 shows the optical microstructure of the deformed Ni-based superalloy at 980 °C and 0.001 s⁻¹. It can be seen that the long needle-shaped δ phases are distorted during hot deformation, and the microvoids appear in the severely deformed parts. Generally, the matrix is seriously softened and the interfacial strength between the matrix and δ phase is significantly weakened at elevated temperature. Thus, the deformation mismatch between the matrix and δ phase results in interface decohesion once the local strain reaches the critical value [38]. Once the interface decohesion occurs, the deformation resistance reduces, and thermally activation process for the dislocation slip is weakened.

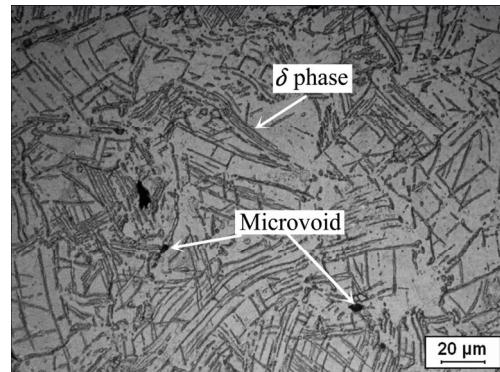


Fig. 13 Optical microstructure of deformed Ni-based superalloy with initial δ phase of 12.09% (deformation temperature: 980 °C; strain rate: 0.001 s⁻¹)

4 Conclusions

1) The effects of initial δ phase on the hot tensile deformation behaviors of the studied Ni-based superalloy are significant. The peak stress increases with the increase of initial δ phase. With the further straining, initial δ phase promotes dynamic softening behaviors, and the flow stress is reduced.

2) Based on the experimental data, the effects of strain and initial content of δ phase on material constants are incorporated into the improved Arrhenius constitutive model. Furthermore, the improved constitutive model can give an accurate and precise estimation of the flow stress over wide ranges of deformation temperature, strain, strain rate and initial δ phase.

3) The apparent activation energy is found in the range of 403.3–480.4 kJ/mol for the studied Ni-based superalloy. The apparent activation energy increases with the increase of initial δ phase. When the initial content of δ phase is 12.09%, the apparent activation energy

decreases with the increase of true strain.

References

- [1] LIN Yong-cheng, CHEN Xiao-min. A critical review of experimental results and constitutive descriptions for metals and alloys in hot processing [J]. *Materials & Design*, 2011, 32(4): 1733–1759.
- [2] CHEN Ming-song, LIN Yong-cheng, MA Xue-song. The kinetics of dynamic recrystallization of 42CrMo steel [J]. *Materials Science and Engineering A*, 2012, 556: 260–266.
- [3] WANG Ming-liang, JIN Pei-peng, WANG Jin-hui, HAN Li. Hot deformation behavior of as-quenched 7005 aluminum alloy [J]. *Transactions of Nonferrous Metals Society of China*, 2014, 24(9): 2796–2804.
- [4] QIN Chun, YAO Ze-kun, NING Yong-quan, SHI Zhi-feng, GUO Hong-zhen. Hot deformation behavior of TC11/Ti–22Al–25Nb dual-alloy in isothermal compression [J]. *Transactions of Nonferrous Metals Society of China*, 2015, 25(7): 2195–2205.
- [5] WEN Dong-xu, LIN Yong-cheng, CHEN Jian, CHEN Xiao-min, ZHANG Jin-long, LIANG Ying-jie, LI Lei-ting. Work-hardening behaviors of typical solution-treated and aged Ni-based superalloys during hot deformation [J]. *Journal of Alloys and Compounds*, 2015, 618: 372–379.
- [6] LI Luo-xing, WANG Guan, LIU Jie, YAO Zai-qi. Flow softening behavior and microstructure evolution of Al–5Zn–2Mg aluminum alloy during dynamic recovery [J]. *Transactions of Nonferrous Metals Society of China*, 2014, 24(1): 42–48.
- [7] QUAN Guo-zheng, LUO Gui-chang, LIANG Jian-ting, WU Dong-sen, MAO An, LIU Qing. Modelling for the dynamic recrystallization evolution of Ti–6Al–4V alloy in two-phase temperature range and a wide strain rate range [J]. *Computational Materials Science*, 2015, 97: 136–147.
- [8] LIN Yong-cheng, CHEN Ming-song, ZHONG Jue. Constitutive modeling for elevated temperature flow behavior of 42CrMo steel [J]. *Computational Materials Science*, 2008, 42(3): 470–477.
- [9] REN Fa-cai, CHEN Jun, CHEN Fei. Constitutive modeling of hot deformation behavior of X20Cr13 martensitic stainless steel with strain effect [J]. *Transactions of Nonferrous Metals Society of China*, 2014, 24(5): 1407–1413.
- [10] GAO Fei, LIU Zhen-yu, MISRA R D K, LIU Hai-tao, YU Fu-xiao. Constitutive Modeling and dynamic softening mechanism during hot deformation of an ultra-pure 17%Cr ferritic stainless steel stabilized with Nb [J]. *Metals and Materials International*, 2014, 20(5): 939–951.
- [11] CAO Y, DI H S, MISRA R D K, ZHANG J C. Hot deformation behavior of alloy 800H at intermediate temperatures: Constitutive models and microstructure analysis [J]. *Journal of Materials Engineering and Performance*, 2014, 23(12): 4298–4308.
- [12] ZHANG Fei, SHEN Jian, YAN Xiao-dong, SUN Jian-lin, SUN Xiao-long, YANG Yin, LIU Yong. High-temperature flow behavior modeling of 2099 alloy considering strain effects [J]. *Transactions of Nonferrous Metals Society of China*, 2014, 24(3): 798–805.
- [13] GAN Chun-lei, ZHENG Kai-hong, QI Wen-jun, WANG Meng-jun. Constitutive equations for high temperature flow stress prediction of 6063 Al alloy considering compensation of strain [J]. *Transactions of Nonferrous Metals Society of China*, 2014, 24(11): 3486–3491.
- [14] XU Guo-fu, PENG Xiao-yan, LIANG Xiao-peng, LI Xu, YIN Zhi-min. Constitutive relationship for high temperature deformation of Al–3Cu–0.5 Sc alloy [J]. *Transactions of Nonferrous Metals Society of China*, 2013, 23(6): 1549–1555.
- [15] TALI M Z, MAZINANI M, FERDOWSI M R G, EBRAHIMI G R, MARVI-MASHHADI M. Strain-dependent constitutive modelling of AZ80 magnesium alloy containing 0.5 wt% rare earth elements and evaluation of its validation using finite element method [J]. *Metals and Materials International*, 2014, 20(6): 1073–1083.
- [16] LIAO Ching-hao, WU Horng-yu, WU Cheng-tao, ZHU Feng-jun, LEE Shyong. Hot deformation behavior and flow stress modeling of annealed AZ61 Mg alloys [J]. *Progress in Natural Science: Materials International*, 2014, 24(3): 253–265.
- [17] WU Horng-yu, YANG Jie-chen, ZHU Feng-jun, WU Cheng-tao. Hot compressive flow stress modeling of homogenized AZ61 Mg alloy using strain dependent constitutive equations [J]. *Materials Science and Engineering A*, 2013, 574: 17–24.
- [18] LI Yu-fei, WANG Zhen-hong, ZHANG Lin-ying, LUO Chao, LAI Xin-chun. Arrhenius-type constitutive model and dynamic recrystallization behavior of V–5Cr–5Ti alloy during hot compression [J]. *Transactions of Nonferrous Metals Society of China*, 2015, 25(6): 1889–1900.
- [19] HE An, XIE Gan-lin, ZHANG Hai-long, WANG Xi-tao. A comparative study on Johnson–Cook, modified Johnson–Cook and Arrhenius-type constitutive models to predict the high temperature flow stress in 20CrMo alloy steel [J]. *Materials & Design*, 2013, 52: 677–685.
- [20] SALARI S, NADERI M, BLECK W. Constitutive modeling during simultaneous forming and quenching of a boron bearing steel at high temperatures [J]. *Journal of Materials Engineering and Performance*. 2015, 24(2): 808–815.
- [21] ABBASI-BANI A R, ZAREI-HANZAKI A, PISHBIN M H, HAGHDADI N. A comparative study on the capability of Johnson–Cook and Arrhenius-type constitutive equations to describe the flow behavior of Mg–6Al–1Zn alloy [J]. *Mechanics of Materials*, 2014, 71: 52–61.
- [22] LI Hui-ping, HE Lian-fang, ZHAO Guo-quan, ZHANG Lei. Constitutive relationships of hot stamping boron steel B1500HS based on the modified arrhenius and Johnson–Cook model [J]. *Materials Science and Engineering A*, 2013, 580: 330–348.
- [23] LIN Yong-cheng, LI Qi-fei, XIA Yu-chi, LI Lei-ting. A phenomenological constitutive model for high temperature flow stress prediction of Al–Cu–Mg alloy [J]. *Materials Science and Engineering A*, 2012, 534: 654–662.
- [24] SHAMSOLHODAEI A, ZAREI-HANZAKI A, GHAMBARI M, MOEMENI S. The high temperature flow behavior modeling of NiTi shape memory alloy employing phenomenological and physical based constitutive models: A comparative study [J]. *Intermetallics*, 2014, 53: 140–149.
- [25] HE An, XIE Gan-lin, ZHANG Hai-long, WANG Xi-tao. A modified Zerilli–Armstrong constitutive model to predict hot deformation behavior of 20CrMo alloy steel [J]. *Materials & Design*, 2014, 56: 122–127.
- [26] CHAI Rong-xia, SU Wen-bin, GUO Cheng, ZHANG Fa-fu. Constitutive relationship and microstructure for 20CrMnTiH steel during warm deformation [J]. *Materials Science and Engineering A*, 2012, 556: 473–478.
- [27] SAMANTARAY D, PATEL A, BORAH U, ALBERT S K, BHADURI A K. Constitutive flow behavior of IFAC-1 austenitic stainless steel depicting strain saturation over a wide range of strain rates and temperatures [J]. *Materials & Design*, 2014, 56: 565–571.
- [28] LIN Yong-cheng, CHEN Xiao-min, WEN Dong-xu, CHEN Ming-song. A physically-based constitutive model for a typical Ni-based superalloy [J]. *Computational Materials Science*, 2014, 83: 282–289.
- [29] LIN Yong-cheng, CHEN Ming-song, ZHONG Jue. Prediction of 42CrMo steel flow stress at high temperature and strain rate [J]. *Mechanics Research Communications*, 2008, 35(3): 142–150.
- [30] JI Guo-liang, LI Qiang, LI Lei. A physically based constitutive relation to predict flow stress for Cu–0.4Mg alloy during hot working [J]. *Materials Science and Engineering A*, 2014, 615:

- 247–254.
- [31] SAJADIFAR S V, YAPICI G G. Elevated temperature mechanical behavior of severely deformed titanium [J]. *Journal of Materials Engineering and Performance*, 2014, 23(5): 1834–1844.
- [32] LIANG Hou-quan, GUO Hong-zhen, NAN Yang, QIN Chun, PENG Xiao-na, ZHANG Jing-li. The construction of constitutive model and identification of dynamic softening mechanism of High-temperature deformation of Ti–5Al–5Mo–5V–1Cr–1Fe alloy [J]. *Materials Science and Engineering A*, 2014, 615: 42–50.
- [33] JAHANGIRI M R, ARABI H, BOUTORABI S M A. Comparison of microstructural stability of IN939 superalloy with two different manufacturing routes during long-time aging [J]. *Transactions of Nonferrous Metals Society of China*, 2014, 24(6): 1717–1729.
- [34] ZHANG Chi, ZHANG Li-wen, LI Meng-fei, SHEN Wen-fei, GU Sen-dong. Effects of microstructure and γ' distribution on the hot deformation behavior for a powder metallurgy superalloy FGH96 [J]. *Journal of Materials Research*, 2014, 29(23): 2799–2808.
- [35] ZHANG Hong-bin, ZHANG Kai-feng, JIANG Shao-song, LU Zhen. The dynamic recrystallization evolution and kinetics of Ni–18.3Cr–6.4Co–5.9W–4Mo–2.19Al–1.16Ti superalloy during hot deformation [J]. *Journal of Materials Research*, 2015, 30: 1029–1041.
- [36] ZHANG Hong-bin, ZHANG Kai-feng, ZHOU Hai-ping, LU Zhen, ZHAO Chang-hong, YANG Xiao-li. Effect of strain rate on microstructure evolution of a nickel-based superalloy during hot deformation [J]. *Materials and Design*, 2015, 80: 51–62.
- [37] LIN Yong-cheng, DENG Jiao, JIANG Yu-qiang, WEN Dong-xu, LIU Guan. Hot tensile deformation behaviors and fracture characteristics of a typical Ni-based superalloy [J]. *Materials & Design*, 2014, 55: 949–957.
- [38] WEN Dong-xu, LIN Yong-cheng, CHEN Jian, DENG Jiao, CHEN Xiao-min, ZHANG Jin-long, HE Min. Effects of initial aging time on processing map and microstructures of a nickel-based superalloy [J]. *Materials Science and Engineering A*, 2015, 620: 319–332.
- [39] LIN Yong-cheng, DENG Jiao, JIANG Yu-qiang, WEN Dong-xu, LIU Guan. Effects of initial δ phase on hot tensile deformation behaviors and fracture characteristics of a typical Ni-based superalloy [J]. *Materials Science and Engineering A*, 2014, 598: 251–262.
- [40] WEN Dong-xu, LIN Yong-cheng, LI Hong-bin, CHEN Xiao-min, DENG Jiao, LI Lei-ting. Hot deformation behavior and processing map of a typical Ni-based superalloy [J]. *Materials Science and Engineering A*, 2014, 591: 183–192.
- [41] LIU Yan-xing, LIN Yong-cheng, LI Hong-bin, WEN Dong-xu, CHEN Xiao-min, CHEN Ming-song. Study of dynamic recrystallization in a Ni-based superalloy by experiments and cellular automaton model [J]. *Materials Science and Engineering A*, 2015, 626: 432–440.
- [42] ZHANG Peng, HU Chao, DING Chao-gang, ZHU Qiang, QIN He-yong. Plastic deformation behavior and processing maps of a Ni-based superalloy [J]. *Materials & Design*, 2015, 65: 575–584.
- [43] ISO 6892-2: Metallic materials-tensile testing-part 2: Method of Test at elevated temperature [S].
- [44] LIN Yong-cheng, HE Min, ZHOU Mi, WEN Dong-xu, CHEN Jian. New constitutive model for hot deformation behaviors of Ni-based superalloy considering the effects of initial δ phase [J]. *Journal of Materials Engineering and Performance*, 2015, 24(9): 3527–3538.
- [45] MIRZADEH H, ROOSTAEI M, PARSA M H, MAHMUDI R. Rate controlling mechanisms during hot deformation of Mg–3Gd–1Zn magnesium alloy: Dislocation glide and climb, dynamic recrystallization, and mechanical twinning [J]. *Materials & Design*, 2015, 68: 228–231.
- [46] QUAN Guo-zheng, LI Gui-sheng, CHEN Tao, WANG Yi-xin, ZHANG Yan-wei, ZHOU Jie. Dynamic recrystallization kinetics of 42CrMo steel during compression at different temperatures and strain rates [J]. *Materials Science and Engineering A*, 2011, 528: 4643–4651.
- [47] LIANG Hou-quan, GUO Hong-zhen, NING Yong-quan, PENG Xiao-na, QIN Chun, SHI Zhi-feng, NAN Yang. Dynamic recrystallization behavior of Ti–5Al–5Mo–5V–1Cr–1Fe alloy [J]. *Materials & Design*, 2014, 63: 798–804.
- [48] KASHYAP B P, CHATURVEDI M C. Activation energy for superplastic deformation of IN718 superalloy [J]. *Scripta materialia*, 2000, 43: 429–433.
- [49] MOMENI A, ABBASI S M. On the opposition of dynamic recrystallization and solute dragging in steels [J]. *Journal of Alloys and Compounds*, 2015, 622: 318–326.

初始 δ 相(Ni₃Nb)对镍基合金高温拉伸变形行为及材料参数的影响

蔺永诚^{1,2,3}, 何敏^{1,3}, 陈明松^{1,3}, 温东旭^{1,3}, 陈荐⁴

1. 中南大学 机电工程学院, 长沙 410083;
2. 中南大学 轻合金研究院, 长沙 410083;
3. 中南大学 高性能复杂制造国家重点实验室, 长沙 410083;
4. 长沙理工大学 能源与动力工程学院 能源高效清洁利用实验室, 长沙 410114

摘要: 通过高温拉伸实验研究了初始 δ 相(Ni₃Nb)含量对一种镍基合金高温拉伸变形行为和材料参数的影响。研究表明, 初始 δ 相含量、变形温度、应变速率和应变对镍基合金高温拉伸变形行为的影响十分显著。基于实验结果, 建立了一种修正的 Arrhenius 本构模型, 其模型的材料参数表达为初始 δ 相含量和应变的函数关系。该模型可以描述初始 δ 相含量、变形温度、应变速率和应变对镍基合金高温拉伸变形行为的综合影响。通过比较, 模型预测值与实验值吻合, 证实了建立的本构模型可精确地预测镍基合金的高温拉伸变形行为。

关键词: 镍基合金; 热变形; 初始 δ 相; 本构模型; 材料参数

(Edited by Yun-bin HE)